Osteoporos Int (2010) 21:81–87
DOI 10.1007/s00198-009-0949-3

ORIGINAL ARTICLE

A longitudinal Raman microspectroscopic study of osteoporosis induced by spinal cord injury

J. Shen · L. Fan · J. Yang · A. G. Shen · J. M. Hu

Received: 6 November 2008 / Accepted: 27 March 2009 / Published online: 13 May 2009
© International Osteoporosis Foundation and National Osteoporosis Foundation 2009

Abstract
Introduction A longitudinal study was established to investigate bone compositional information in spinal cord injury (SCI) rat model.
Methods Raman spectroscopy was applied to detect the distal femur and humeri of SCI, sham-operated (SO), and age-matched control (CON) male Sprague-Dawley (SD) rats at first, second, third, and fifth weeks after surgery. One-way ANOVA and Tukey's HSD post hoc multiple comparison tests were used to analyze the longitudinal data of mineral to matrix ratio and carbonate substitution.
Results Relative mineral decrease was found in SCI group by more than 20% in femur and approximately 12% in humeri compared with CON group. No significant changes in carbonate substitution were observed.
Conclusions Severe bone loss in the early stage of SCI was confirmed by a continuous decrease of the mineral to collagen matrix ratio. The decrease in the humeri suggested hormone level variations might participate in the etiology of SCI-induced osteoporosis.

Keywords Carbonation · Mineral to matrix ratio · Osteoporosis · Raman spectroscopy · Spinal cord injury

J. Shen · J. Yang · A. G. Shen (✉) · J. M. Hu (✉)
College of Chemistry and Molecular Sciences, Wuhan University, Wuhan, Hubei 430072, People's Republic of China
e-mail: agshen@whu.edu.cn
e-mail: jmhu@whu.edu.cn

L. Fan
Department of Orthopedics, Renmin Hospital, Wuhan University, Wuhan, People's Republic of China

Introduction

Osteoporosis, almost an inevitable consequence of spinal cord injury (SCI), occurs predominantly in sublesional sites [1–3]. Continuous bone loss leads to increased bone fragility and risk of spontaneous fracture [4]. Many factors should be taken into consideration in SCI-induced osteoporosis, such as age, sex, injury grade, and duration after injury. Bone loss after SCI distinguishes itself from the other osteoporosis etiologies by its more rapid and severe reduction in bone mineral density (BMD). For instance, it was reported that SCI induced more deterioration than bed rest, sciatic neurectomy, ovariectomy, and etc [5–7].

The measurement of BMD is commonly considered to be a gold standard for the assessment of bone loss [8, 9], but it is estimated to explain only 50~80% of the variance in bone strength [10, 11]. The results for individuals with or without fracture are somehow overlapping [12, 13]. Although dual energy X-ray absorptiometry (DXA) is the most conventional method for osteoporosis detection, it can only give planar information while micro-computed tomography (CT) provides three-dimensional (3D) architecture information which illustrates additional character of bone quality [5]. Scanning electron microscopy (SEM) and transmission electron microscopy (TEM) were also applied in the study of bone structure at micro- and nano-scales [14, 15]. These common methods that can be adopted to investigate hierarchical structure of bone at different levels of organization are easy to apply and most of them are non-destructive. However, all of them focus on structural and morphologic domain and cannot detect compositional information which is also vital to bone quality. Raman spectroscopy is a well-established analytical tool which is based on the interaction of electromagnetic radiation with the molecules in the samples. It has been widely used in

biomedical field in recent decades [16, 17] owing to its versatility for various samples in which hydrated tissue specimens are also included since water contributes slightly to the spectrum. In addition, Raman spectroscopy can provide simultaneous information of organic and inorganic constituents of samples with micro-level spatial resolution. In 1970s, the method was introduced into the study of bones [18] and ever since then emerged as an important complement to traditional methods in this domain [19, 20]. For example, different mineral crystallites and substitution can be easily distinguished by Raman spectroscopy [21, 22]. The method also proved that mechanical damage ranging from microcracks to overt fracture caused permanent structural changes to mineral crystallites, including formation of local regions of uncarbonated apatite [23]. Studies using Raman spectroscopy have found compositional differences not only in women with and without osteoporotic fracture, but in mature intact and ovariectomized monkeys [24, 25].

Although various researches were conducted in the study of SCI-induced osteoporosis, most of them focused on structural changes. The current study intended to explore whether compositional changes occur after SCI besides deterioration of bone structure such as trabecular number, density, and thickness. This may contribute to the explanation of the mechanism of SCI-induced osteoporosis which is complicated and remains controversial. In the present study, we discussed the possible participation of hormone regulation in the pathophysiology of humeri mineral to matrix decrease. Raman spectroscopy was applied to obtain molecular information of femur and humeri of Sprague-Dawley (SD) rats after spinal cord transection. The compositional information of trabecular region was accessed at different time points in the first, second, third, and fifth week after the surgery. The purpose of this research is to establish a longitudinal study of bone compositional changes in the SCI model. It was hypothesized that besides morphological changes, compositional changes took place after SCI in a certain duration of time.

Materials and methods

Animal protocols

The experiments were performed according to the Animal Welfare and Ethical Review Committees and the Principles of Laboratory Animal Care (NIH publication No. 80-23, revised 1996) were followed.

Seventy-two male SD rats (7 weeks of age, 200±20 g of weight) were randomly assigned into three groups: the spinal cord injury (SCI) group, the sham-operated (SO) group, and the age-matched control (CON) group. There were 24 rats in each group. All rats were housed in the animal research facility (Renmin Hospital, Wuhan University, China) at controlled temperature (24±1°C) and humidity (60~65%) under a standard 12 h/12 h light–dark cycle, with free access to food and water. Rats in the SCI group were anesthetized by intraperitoneal injection of pentobarbital sodium (40 mg/kg, i.p.). Later an incision was made at the back and laminectomy was applied to expose the lower thoracic cord at $T_{10–12}$ segments. Then the spinal cord was transected with fine scissors. Finally, the surgical wound was closed in two layers. The urinary bladder of the SCI rats was emptied manually until spontaneous micturition recovered. Rats in SO group underwent the same surgery except for the transecting of spinal cord. After surgery rats in SCI group ambulated by dragging their hindlimbs while rats in SO group ambulated with all limbs. Animals were sacrificed and perfused through the ascending aorta with 200 ml of 0.9% physiological saline after 1, 2, 3, and 5 weeks of feeding, each time six rats in each group. Left femora and humeri were harvested with careful removal of adhesive soft tissues, and then stored at –80°C immediately. Femora and humeri were cut along the axis of the diaphysis through condyle and caput with a low-speed spindle. Since flat surface reflects more Raman scattering light, the cross-section was cautiously polished using a graded series of grits, followed by 0.3 μm alumina slurry. The specimens were sonicated briefly to remove any particles that absorbed on the specimens. Samples were soaked in physiological saline for 12 h under 4°C before Raman measurements.

Raman spectroscopy

Raman spectra were obtained with HR800 Raman microspectroscopy (Jobin Yvon, France). A 632.8-nm He–Ne laser was focused onto the specimen using a ×50/0.5 NA objective (Olympus, Japan). The laser beam around 1.5 μm in diameter was focused on specimens. A 600 g/mm grating provided a spectral dispersion of about 1 cm^{-1}/pixel. The entrance slit was set at 80 μm. For each scan the integration time was 20 s and the final spectrum of each spot was the average of six scans. The spectral resolution was 1.12 cm^{-1} and the wave number range from 300 cm^{-1} to 1,900 cm^{-1} was covered. All measurements were made at room temperature (24±1°C). Data were acquired with the LabSpec software (Jobin Yvon, France). To evaluate compositional homogeneity, Raman mapping areas of 10×10 and 40×40 μm^2 were detected at epiphysis and metaphysis of distal femur and caput of humerus. The step was set to 1 and 4 μm for 10×10 and 40×40 μm^2 area

separately. For single spectrum detection, 25 separate spots were obtained randomly on trabecular region at each of the mentioned parts on the sample.

Data analysis

Sample background subtraction was accomplished using the LabSpec software. Intensities of specific peaks were exported; the mineral to matrix ratio and the carbonate substitution were calculated. Since the intensity ratio of certain peaks is proportional to the relative amounts of the related species in vibrational spectroscopy, two intensity ratios were selected to describe the degree of relative mineral content and the extent of type B carbonate substitution, respectively. The predominant sharp peak at ~960 cm^{-1} is the symmetrical stretching υ_1 band of PO_4^{3-}. It is influenced to a minor extent by environmental factors than the other phosphate vibrational modes. Therefore, it is the most proper band to evaluate phosphate level among the four vibrational modes of PO_4^{3-}. Actually, the degree of relative mineral content was determined by the mineral to matrix ratio which was calculated by dividing the intensity of phosphate symmetric stretch band (at ~960 cm^{-1}) with carbon skeletal stretch band (at ~1,451 cm^{-1}). The extent of type B carbonate substitution was quantified by dividing the intensity of phosphate symmetric stretch band (at ~960 cm^{-1}) with the type B carbonate symmetric stretch band (at ~1,072 cm^{-1}). Then the results were analyzed with SPSS software. Data were expressed as the mean ± standard error of the mean. Mean mineral to matrix ratio and mean substitution values were analyzed using one-way analysis of variance (ANOVA) followed by Tukey's HSD post hoc multiple comparison tests. Differences were considered to be statistically significant for $P<0.05$, and all tests were used two-sided.

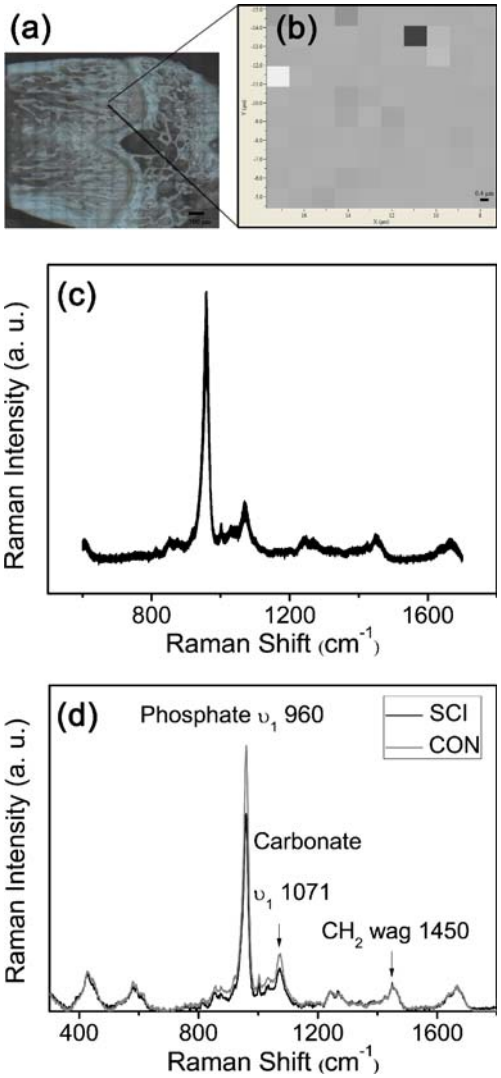

Fig. 1 **a** Section of condyle femur, **b** Raman mapping of 10×10 μm^2 area, with an increment of 1 μm, the mapping is based on the intensity ratio of Raman shift at 960 cm^{-1} and 1,072 cm^{-1}, **c** 100 overlapping spectra from the mapping area mentioned in Fig. 1b, **d** typical Raman spectra of trabeculae for SCI and CON rats

Results

Raman analysis

The section of condylus femoris is shown in Fig. 1a, both epiphysis and metaphysis at the two sides of epiphyseal line were detected by Raman microspectroscopy.

The gray scale of Raman mapping (Fig. 1b) showed the mineral to matrix intensity ratio in the 10×10 μm^2 area. The 'higher intensity ratio' area is labeled with lighter color. Certain homogeneity was observed at the chosen area except for few light or dark dots. All the 100 spectra for the mapping (Fig. 1c) are highly overlapping. Same results were obtained in the chosen area for epiphysis, metaphysis, and caput humeri, respectively. For the 40×40 μm^2 area similar homogeneity were observed for all the detected specimens.

The typical Raman spectra (Fig. 1d) of trabecular bone for CON and SCI groups have the same peak positions, but their intensity at certain Raman shifts are different. The most distinct band at ~960 cm^{-1} is symbolic for mineral content. The intensity at this position for CON group (gray line) is higher than SCI group (black line), which indicates greater amount of mineral content. The vibration of the type B carbonate substitution is at 1,072 cm^{-1}. Raman shift at 1,451 cm^{-1} represents the CH_2 wag vibration, which is associated with the organic component. The assignments of all Raman bands are listed in Table 1.

Table 1 Assignments of Raman spectroscopy of trabeculae (300–1,900 cm^{-1})

Raman shift (cm^{-1})	Assignment
429	υ_2 PO_4^{3-}
584	υ_4 PO_4^{3-}
853	δ (C–C–H)
877	υ (C–C)
960	υ_1 PO_4^{3-}
1,003	υ_3 HPO_4^{2-}
1,034	υ_3 PO_4^{3-}
1,072	CO_3^{2-} υ_1, type B carbonate substitution
1,244	Amide III (random coils)
1,270	Amide III (α-helix)
1,451	CH_2 wag
1,635	Amide I (β-turn)
1,665	Amide I (random coils)

Mineral to matrix ratio

The mineral to matrix ratio for SCI group in metaphysis and epiphysis decreased continuously after surgery (Fig. 2). In the first 3 weeks, the relative mineral decrease in SCI group was more severe with an average rate of 7.2% and 6.5% per week while the average decrease rate for the last 2 weeks were 2.7% and 2.8% per week compared with CON group for metaphysis and epiphysis, respectively. From the first week to the fifth week, the mineral content to the collagen matrix ratio in SCI group has a total decrease of 27% and 25% compared with CON group for metaphysis and epiphysis, respectively. At each time point, trabecular region in SCI group was detected to be less mineralized compared with both CON and SO groups (Tukey's HSD, $P<0.05$). In humeri SCI group also had a decreasing mineral to matrix ratio (Fig. 2), but not as much as in femur. During the 5 weeks after surgery, this ratio in SCI group decreased by 12% compared with CON group. At the first 2 weeks, the mineral to matrix decrease was not significant, but from the third week on, the mineral to matrix decrease became significant compared with CON and SO groups (Tukey's HSD, $P<0.05$).

Carbonation

Despite of the lattice sites it occupied, carbonate substitutions are divided into type A (hydroxyl group), type B (phosphate group) and labile (on the surface) substitution. Raman spectroscopy is only capable of monitoring type B carbonation. The phosphate to carbonate ratio (PO_4^{3-}/CO_3^{2-}) for metaphysis and epiphysis (Fig. 3) stayed almost constant for CON, SO, and SCI groups except for an increase in the fifth week of SCI group compared with the other two groups (Tukey's HSD, $P<0.05$). The difference between SCI group and the other two groups in humeri (Fig. 3) were not significant at all time points.

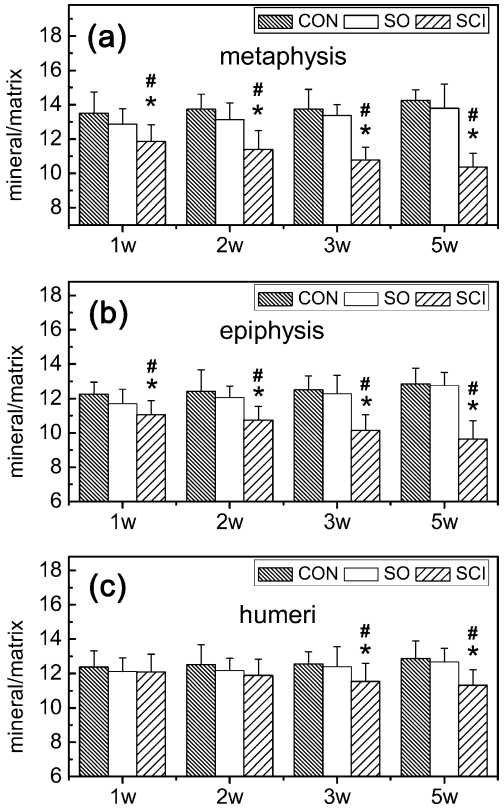

Fig. 2 Mineral to matrix ratio of trabeculae for **a** metaphysis; **b** epiphysis; **c** humeri during the time of 1, 2, 3, and 5 weeks. Spinal cord injury (SCI) group had a lower mineral to matrix ratio than sham-operated (SO) and age-matched control (CON) groups, at fifth week SCI group of metaphysis, epiphysis, and humeri was 27%, 25%, and 12% less than CON group. One-way ANOVA was followed by Tukey's HSD post hoc multiple comparison tests. $^{\#}P<0.05$ vs. the CON group. $^{*}P<0.05$ vs. the SO group

Discussion

The purpose of this study was to investigate the effects of SCI on bone physiochemical composition. To our knowledge, for the first time, the compositional information is provided for SCI-induced osteoporosis. SCI brought significant decrease in the mineral to matrix ratio in the lower extremities, the loss of relative mineral content increased with time. In the upper extremities relative mineral decrease was also observed with a lower degree. However, type B carbonate substitution did not change as significantly as the mineral to matrix ratio in the first 3 weeks, while in the fifth week a significant decrease was observed at metaphysis and epiphysis.

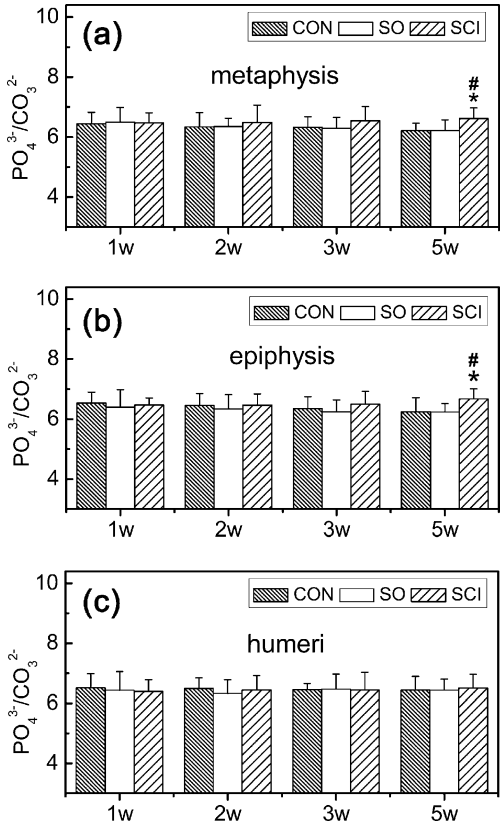

Fig. 3 Carbonate substitution of trabeculae for **a** metaphysis; **b** epiphysis; **c** humeri during the time of 1, 2, 3, and 5 weeks. No significant differences between spinal cord injury (SCI) group and sham-operated (SO), or age-matched control (CON) group exist in the first 3 weeks. Increased phosphate to carbonate ratio (PO_4^{3-}/CO_3^{2-}) was found in the fifth week. One-way ANOVA was followed by Tukey's HSD post hoc multiple comparison tests. $^{\#}P<0.05$ vs. the CON group. $^{*}P<0.05$ vs. the SO group

Bone tissue is complicated with hierarchical structures. Fourier transform infrared imaging (FTIRI) studies showed the heterogeneity of trabeculae chemical composition in the 400×400 μm^2 scale with approximately 6-μm spatial resolution [26, 27]. However, in the 10×10 μm^2 area with 1 μm spatial resolution, our Raman mapping showed certain compositional homogeneity of trabeculae. Hence, Raman spectrum from each single point of trabeculae is representative of the spectroscopic characteristics of the micro-scale area. The single spot equally corresponds to the intrinsic spectroscopic character of 10×10 μm^2 area. Even though it is heterogeneous in larger scale, the average of randomly selected detection spots instead of the mapping of entire cross-section provides adequate information of the whole trabeculae. In this way rapid access can be achieved, which avoids the system uncertainty arising from instrumental drift and photon bleaching due to long-term laser irradiation.

Raman spectroscopic study of osteoporosis after SCI provides information of organic and inorganic components of bone simultaneously, which are not supplied by conventional methods. In comparison with FTIR, Raman spectroscopy provides higher resolution accompanied with less interference from water. The direct compositional information of bone would help to understand how SCI affected bone in physicochemical side, thus further elucidate the mechanism of SCI-induced osteoporosis.

Many reports demonstrated that the trabeculae from SCI patients were fewer and spaced farther apart in the suffering bone than normal bones [1–3]. To get more direct information from the affected bone, Rubin et al. used TEM to detect bone crystals. They reported that there was no substantial difference in length or thickness between normal and osteoporotic bone crystals [15], which suggested that the lower BMD was subject to a reduction in trabecular structure rather than a deterioration of the bone crystals at the nano-scale. At the same time, composition differences between osteoporotic bone and normal bone were detected with spectroscopic methods. In humans and animal models of osteoporosis, diseased bone had a decreased mineral to matrix ratio, which is characteristic of immature bone [28, 29]. Our results confirm and complement the BMD and histological results of bone loss in SCI-induced osteoporosis by showing 27% and 25% relative mineral decrease at metaphysis and epiphysis, respectively. It was reported that calcium and phosphate homeostasis was disordered in SCI patients. The impaired phosphate metabolism arose from the uncoupling bone resorption and formation [30]. In early stage of SCI serum phosphate and ionized calcium significantly increased, so did urinary calcium excretion, which led to an empirical conclusion that the bone mineral phase was released into the blood circulation and outside the body [31, 32]. The severe phosphate content decrease in the affected bone indicated the exceeding resorption by osteoclasts, thereby, it was proved that the increased serum phosphate was definitely endogenous owing to the release of mineral phase from bone tissue. Combination of the clinical results and the direct mineral decrease information from Raman spectroscopy would complete the investigation of phosphate homeostasis in the whole circulation.

Most studies on SCI-induced osteoporosis focused on the loss of bone below trauma. Researches indicated that there were no changes in BMD of trabecular or cortical bone of upper limbs in subjects with paraplegia [2] and even on the contrary, a minor increase of BMD (6%) was reported [33]. However, our results showed that even without structure deterioration, compositional changes took place in the upper limbs. Although compared with the changes in metaphysis and epiphysis, changes in the humeri were fairly less by 12% mineral to matrix decrease, to our knowledge it is the first time we observed relative mineral loss in supralesional bones. Common understanding of the

maintenance or even an increase of BMD in upper limbs is that the upper extremities ambulate freely or they are even used more due to the disabled lower extremities, thus the formation of bone in upper limbs is accelerated. This disuse mechanism is one of the most widely accepted explanations for SCI-induced osteoporosis; other mechanisms for the pathophysiology include denervation and hormonal changes [34]. The fact that there was much more mineral to matrix decrease in the hindlimbs than forelimbs highly supports the disuse hypothesis whereas the mineral to matrix decrease in forelimbs cannot be explained by the same mechanism. Deafferentation of the sympathetic nervous system after SCI compressed gas exchanges and blood nutritive supplies to the bone, thus osteoclast formation and bone resorption were promoted. However, the forelimbs were likewise not affected by neural factors. Except for disuse and denervation, the mineral to matrix decrease in humeri indicates the participation of other mechanisms in the induction of osteoporosis. Certain hormone levels play a pivotal role in regulating bone remodeling, such as parathyroid hormone (PTH), insulin, estrogen, and androgen. [34] The circulating concentrations of these hormones may stimulate or inhibit osteocyte (e.g. osteoblast, osteoclast) precursor formation in the bone marrow and thus affecting the balance of bone formation and resorption. Diverse bone markers were reported to be varied after acute SCI in which bone formation markers had a minor rise while bone resorption markers had a significant rise, in the same study, a decrease of PTH level was observed after 3 weeks [32]. In the therapy of osteoporosis, PTH is distinct from the other conventional antiresorptive agents by stimulating bone formation instead of suppressing bone resorption, within a 7-week therapy BMD increased by 9–17% [35]. Our results with regards to humeri in which mineral to matrix decrease became significant from the third week and continued to the fifth week are somehow coincident with the case mentioned in the above studies. In addition, inhibitory effects on gonadal function which is in close relation to the secretion of estrogen as well as androgen, suppressed vitamin D levels, and depressed insulin level were likewise reported to contribute to the pathogenesis of SCI-induced osteoporosis [34]. We suggest that changes of certain hormone levels which regulate the remodeling of bone possibly contribute to the relative mineral to matrix decrease although we do not have correlative data to prove which kinds of hormone actually brought forth the decrease.

More carbonate substitution indicates more mature bone composition. The substitution of carbonate ions in phosphate positions significantly increased with age [36]. FTIR study of ovariectomized cynomolgus monkeys showed a decrease in B-type carbonate at trabecular bone [37]. Chemical analysis showed that carbonate content of samples from control ovariectomized animals was less than those from normal [28]; however, this is the total carbonate substitution for A-type, B-type, and labile carbonate, not specifically for B-type carbonate. Results in the current study provided only significant increase of the phosphate to carbonate ratio for metaphysis and epiphysis at the fifth week. Since the phosphate to collagen ratio was decreasing, no significant change of this ratio also indicates a decrease of B-type carbonate. This is somehow in accordance with the above literature. At the fifth week, the significant increase of the phosphate to carbonate ratio indicate accelerated loss of carbonate.

Certain limitations should be considered in this study. First of all there is a lack of correlated hormone level data to support the conclusion that hormone level changes lead to the mineral to matrix decrease after SCI. Furthermore, which kinds of hormone exactly induced the decrease still remains unknown. In addition, Bohic et al. found that different techniques produced several inconsistent findings, which demonstrated the difficulty in obtaining reliable, comparable results when analyzing bone minerals by a variety of spectroscopic techniques [28]. Moreover, though Raman spectroscopy is prosperously developing to be an in vivo method in biomedical field, in vivo study for bone is still limited due to its deep location inside the body and the difficulty to get interested signal by eliminating spectral components of overlying tissues. Thus, a repeated study for the same specimen across the time span remains difficult at the moment; this will import individual differences into the results and increase the amount of the demanded animals.

In summary, organic and inorganic compositions were studied simultaneously by micro-Raman spectroscopy; this direct information of bone would help further understand the mechanism of osteoporosis after SCI. The compositional changes in the upper limbs indicated that disuse and denervation were not the only factors leading to osteoporosis, it is suggested that hormone modulation should be taken into account. Correlating studies which detect synchronously hormone level changes would further reveal the relationship between mineral to matrix decrease and hormone levels.

Acknowledgements This work is financially supported by National Natural Science Foundation of China (No. 20705025, No. 30772058).

Conflicts of interest None.

References

1. Kiratli BJ, Smith AE, Nauenberg T et al (2000) Bone mineral and geometric changes through the femur with immobilization due to spinal cord injury. J Rehabil Res Dev 37:225–233

2. Frey-Rindova P, de Bruin ED, Stussi E et al (2000) Bone mineral density in upper and lower extremities during 12 months after spinal cord injury measured by peripheral quantitative computed tomography. Spinal Cord 38:26–32
3. Liu CC, Theodorou DJ, Theodorou SJ et al (2000) Quantitative computed tomography in the evaluation of spinal osteoporosis following spinal cord injury. Osteoporos Int 11:889–896
4. Lazo MG, Shirazi P, Sam M et al (2001) Osteoporosis and risk of fracture in men with spinal cord injury. Spinal Cord 39:208–214
5. Jiang SD, Jiang LS, Dai LY (2006) Spinal cord injury causes more damage to bone mass, bone structure, biomechanical properties and bone metabolism than sciatic neurectomy in young rats. Osteoporos Int 17:1552–1561
6. Jiang SD, Shen C, Jiang LS et al (2007) Differences of bone mass and bone structure in osteopenic rat models caused by spinal cord injury and ovariectomy. Osteoporos Int 18:743–750
7. Bieringsorensen F, Bohr H, Schaadt O (1988) Bone-mineral content of the lumbar spine and lower-extremities years after spinal-cord lesion. Paraplegia 26:293–301
8. Siris ES, Brenneman SK, Miller PD et al (2004) Predictive value of low BMD for 1-year fracture outcomes is similar for postmenopausal women ages 50–64 and 65 and older: results from the National Osteoporosis Risk Assessment (NORA). J Bone Miner Res 19:1215–1220
9. Poetzschner R, Abendroth K (2001) Relationship of risk factors, clinical and X-ray findings of osteoporosis with BMD results of different QCT and pQCT measurements. J Bone Miner Res 16 (suppl):518–518
10. Carter DR, Hayes WC (1977) Compressive behavior of bone as a 2-phase porous structure. J Bone Joint Surg Am 59:954–962
11. Majumdar S, Kothari M, Augat P et al (1998) High-resolution magnetic resonance imaging: three-dimensional trabecular bone architecture and biomechanical properties. Bone 22:445–454
12. Lee C, Almagor O, Dunlop DD et al (2007) Self-reported fractures and associated factors in women with systemic lupus erythematosus. J Rheumatol 34:2018–2023
13. Bolotin HH (2007) DXA in vivo BMD methodology: an erroneous and misleading research and clinical gauge of bone mineral status, bone fragility, and bone remodelling. Bone 41:138–154
14. Rubin MA, Rubin J, Jasiuk I (2004) SEM and TEM study of the hierarchical structure of C57BL/6J and C3H/HeJ mice trabecular bone. Bone 35:11–20
15. Rubin MA, Jasiuk I, Taylor J et al (2003) TEM analysis of the nanostructure of normal and osteoporotic human trabecular bone. Bone 33:270–282
16. Barbosa CJ, Vaillancourt FH, Eltis LD et al (2002) The power distribution advantage of fiber-optic coupled ultraviolet resonance Raman spectroscopy for bioanalytical and biomedical applications. J Raman Spectrosc 33:503–510
17. Vo-Dinh T, Yan F, Wabuyele MB (2006) Surface-enhanced Raman scattering for biomedical diagnostics and molecular imaging. In: Kneipp K, Moskovits M, Kneipp H (eds) Surface-enhanced Raman scattering: physics and applications. Springer, Berlin, pp 409–426
18. Walton AG, Deveney MJ, Koenig JL (1970) Raman spectroscopy of calcified tissue. Calcif Tissue Res 6:162–167
19. Draper ERC, Morris MD, Camacho NP et al (2005) Novel assessment of bone using time-resolved transcutaneous Raman spectroscopy. J Bone Miner Res 20:1968–1972
20. Penel G, Delfosse C, Descamps M et al (2005) Composition of bone and apatitic biomaterials as revealed by intravital Raman microspectroscopy. Bone 36:893–901
21. Penel G, Leroy N, Van Landuyt P et al (1999) Raman microspectrometry studies of brushite cement: in vivo evolution in a sheep model. Bone 25(suppl):81–84
22. Weiner S (2006) Transient precursor strategy in mineral formation of bone. Bone 39:431–433
23. Carden A, Rajachar RM, Morris MD et al (2003) Ultrastructural changes accompanying the mechanical deformation of bone tissue: a Raman imaging study. Calcif Tissue Int 72:166–175
24. McCreadie BR, Morris MD, Chen TC et al (2006) Bone tissue compositional differences in women with and without osteoporotic fracture. Bone 39:1190–1195
25. Gadeleta SJ, Boskey AL, Paschalis E et al (2000) A physical, chemical, and mechanical study of lumbar vertebrae from normal, ovariectomized, and nandrolone decanoate-treated cynomolgus monkeys (*Macaca fascicularis*). Bone 27:541–550
26. Faibish D, Gomes A, Boivin G et al (2005) Infrared imaging of calcified tissue in bone biopsies from adults with osteomalacia. Bone 36:6–12
27. Ou-Yang H, Paschalis EP, Mayo WE et al (2001) Infrared microscopic imaging of bone: spatial distribution of CO_3^{2-}. J Bone Miner Res 16:893–900
28. Bohic S, Rey C, Legrand A et al (2000) Characterization of the trabecular rat bone mineral: effect of ovariectomy and bisphosphonate treatment. Bone 26:341–348
29. Paschalis EP, Betts F, DiCarlo E et al (1997) FTIR microspectroscopic analysis of human iliac crest biopsies from untreated osteoporotic bone. Calcif Tissue Int 61:487–492
30. Jiang SD, Dai LY, Jiang LS (2006) Osteoporosis after spinal cord injury. Osteoporos Int 17:180–192
31. Maimoun L, Couret I, Micallef JP et al (2002) Use of bone biochemical markers with dual-energy X-ray absorptiometry for early determination of bone loss in persons with spinal cord injury. Metabolism 51:958–963
32. Roberts D, Lee W, Cuneo RC et al (1998) Longitudinal study of bone turnover after acute spinal cord injury. J Clin Endocrinol Metab 83:415–422
33. Dauty M, Verbe BP, Maugars Y et al (2000) Supralesional and sublesional bone mineral density in spinal cord-injured patients. Bone 27:305–309
34. Jiang SD, Jiang LS, Dai LY (2006) Mechanisms of osteoporosis in spinal cord injury. Clin Endocrinol 65:555–565
35. Iida-Klein A, Hughes C, Lu SS et al (2006) Effects of cyclic versus daily hPTH(1–34) regimens on bone strength in association with BMD, biochemical markers, and bone structure in mice. J Bone Miner Res 21:274–282
36. Akkus O, Adar F, Schaffler MB (2004) Age-related changes in physicochemical properties of mineral crystals are related to impaired mechanical function of cortical bone. Bone 34:443–453
37. Huang RY, Miller LM, Carlson CS et al (2003) In situ chemistry of osteoporosis revealed by synchrotron infrared microspectroscopy. Bone 33:514–521